Available online at www.sciencedirect.com

ScienceDirect

Biochimica et Biophysica Acta 1758 (2006) 846–857

BIOCHIMICA ET BIOPHYSICA ACTA

BBA

www.elsevier.com/locate/bbamem

Review

Chemical imaging of biological tissue with synchrotron infrared light

Lisa M. Miller [a,*], Paul Dumas [b]

[a] National Synchrotron Light Source, Bldg. 725 D, Brookhaven National Laboratory, 75 Brookhaven Avenue, Upton, NY 11973, USA
[b] SOLEIL Synchrotron, L'Orme des Merisiers, Saint-Aubin- BP 48, 91192 Gif-sur-Yvette Cedex, France

Received 26 January 2006; received in revised form 30 March 2006; accepted 10 April 2006
Available online 21 April 2006

Abstract

Fourier transform infrared micro-spectroscopy (FTIRM) and imaging (FTIRI) have become valuable techniques for examining the chemical makeup of biological materials by probing their vibrational motions on a microscopic scale. Synchrotron infrared (S-IR) light is an ideal source for FTIRM and FTIRI due to the combination of its high brightness (i.e., flux density), also called brilliance, and broadband nature. Through a 10-μm pinhole, the brightness of a synchrotron source is 100–1000 times higher than a conventional thermal (globar) source. Accordingly, the improvement in spatial resolution and in spectral quality to the diffraction limit has led to a plethora of applications that is just being realized. In this review, we describe the development of synchrotron-based FTIRM, illustrate its advantages in many applications to biological systems, and propose some potential future directions for the technique.

Keywords: Synchrotron; Infrared; Microspectroscopy; Imaging; Biology; Biomedical

Contents

Abbreviations: IR, infrared; FTIRM, Fourier transform infrared microspectroscopy; FTIRI, Fourier transform infrared imaging; FPA, focal plane array; MCT, mercury cadmium telluride; S/N, signal-to-noise; S-IR, synchrotron infrared

* Corresponding author. Tel.: +1 631 344 2091; fax: +1 631 344 3238.
E-mail address: lmiller@bnl.gov (L.M. Miller).

0005-2736/$ - see front matter © 2006 Elsevier B.V. All rights reserved.
doi:10.1016/j.bbamem.2006.04.010

1. Introduction

Fourier transform infrared micro-spectroscopy (FTIRM) and imaging (FTIRI) are techniques that combine light microscopy and infrared spectroscopy. Light microscopy is used to magnify structural detail in samples, while infrared spectroscopy provides information on molecular chemistry. Together, chemical analysis can be performed with microscopic detail.

FTIRM was developed over 20 years ago using a conventional thermal (e.g., globar) infrared light source and a single-element infrared (IR) detector. It has been used to identify and spatially resolved the chemical makeup of many diverse materials, including various plant and animal tissues, minerals and other geological samples, polymers films and laminates, semiconductors, forensics materials, and pharmaceuticals [1].

FTIRI is a relatively new term associated with the recent development of focal plane array (FPA) detectors on IR microscopes [2,3]. The FPA detector consist of an array of IR detector elements that enable spectra of various parts of the sample to be projected on different pixels and collected simultaneously, while the concurrent measurement of all frequencies is retained by the phase modulation of the interferometer. Using a FPA system, the speed at which large IR images can be collected is dramatically improved.

When examining the chemical makeup of biological cells and tissues with an IR microscope, it is important to achieve sub-cellular spatial resolution. For both FTIRM and FTIRI, the spatial resolution is limited by the wavelengths of IR light, which are longer than visible light wavelengths used for conventional optical microscopy. The diffraction-limited spatial resolution is dependent upon the wavelength of light and the numerical aperture (NA) of the focusing optic [4]. Typical IR microscopes utilize Schwarzschild objectives with a NA of ~0.6. In an FTIRM experiment, apertures confine the beam to the sample's area of interest. Some microscopes utilize a single aperture before the sample, which controls the region illuminated. With a single aperture, the diffraction-limited spatial resolution is approximately $2\lambda/3$ [5]. Thus for the mid-IR range, the diffraction-limited spatial resolution is approximately 1.7 μm (at 4000 cm^{-1}) to 13 μm (at 500 cm^{-1}). Other microscopes operate in a confocal arrangement, where a second aperture is used after the sample to define the region being sensed by the IR detector. For such a confocal microscope, where objectives and apertures are placed both before and after the sample, the spatial resolution is improved to $\sim\lambda/2$ [5]. In addition, the confocal arrangement also reduces the Schwarzschild's first- and higher-order diffraction rings, dramatically improving image contrast [5].

In an FTIRI experiment, no physical apertures are used to limit the illumination area of the IR beam. Instead, an array of IR detector elements is used to collect the projected image of the unmasked IR beam on the sample. While FPA systems dramatically improve the rate at which IR images can be collected, the spatial resolution is not as good as a confocal FTIRM microscope because an FTIRI instrument cannot operate in a confocal arrangement.

2. Advantages of a synchrotron IR source

In an FTIRM experiment, as the aperture size is decreased, so does the IR flux that reaches the detector. Hence, the S/N decreases. A conventional globar source illuminates light into a ~100 μm area, so typical aperture settings are 20–100 μm.

A synchrotron infrared source is 100–1000 times brighter than a conventional thermal (e.g., globar) source [6]. This brightness advantage is not because the synchrotron produces more power, but because the effective source size is small and the light is emitted into a narrow range of angles. The high brightness (i.e., flux density) of the synchrotron source allows smaller regions to be probed with acceptable signal-to-noise [7,8]. A synchrotron IR source typically fills a 10–20 μm area. Thus, a synchrotron source provides no advantage over the thermal source for larger aperture settings (~20 μm or greater). Fig. 1A demonstrates the difference in brightness between a synchrotron and globar source by comparing the throughput as a function of aperture size [9]. As can be seen for example, the globar source transmits very little light through a 10-μm aperture, whereas >80% of the synchrotron IR light passes through the same size aperture. However, with a 70-μm aperture, the synchrotron source provides no advantage. Fig. 1B shows the

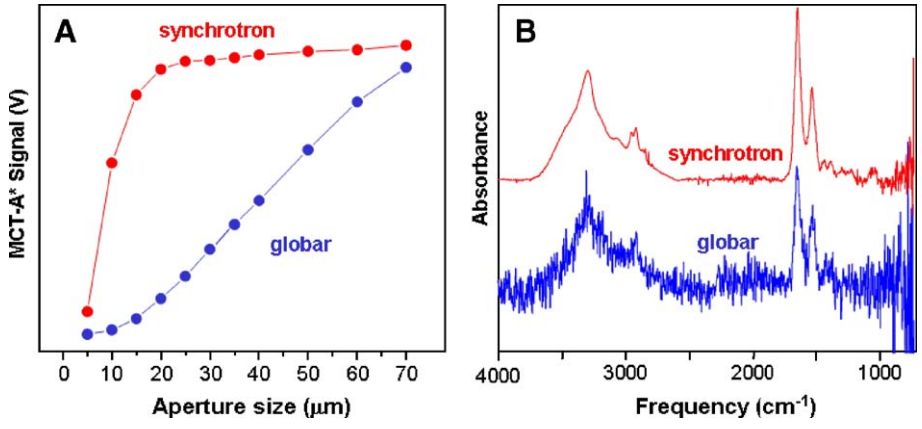

Fig. 1. (A) Infrared signal through various aperture sizes using a synchrotron versus globar source. A confocal IR microscope was used with a single-point detector. (B) Infrared spectra of a single red blood cell collected with a synchrotron versus globar source. A square aperture of 5×5 μm was used.

infrared spectra of a single red blood cell collected with a 5×5 μm square aperture, illustrating how the brightness advantage of the synchrotron leads to dramatically improved S/N.

In addition to its high brightness, synchrotron IR light has other advantages of over the conventional thermal source: it has a pulsed time structure and a high degree of polarization (when a bending magnet is used for producing the IR photons). The pulsed nature of the light comes from the intrinsic characteristics of synchrotron radiation, where the specific pulse structure (10 s to 100 s of picoseconds) is determined by the electron bunch structure in the storage ring [10]. The polarization of the synchrotron IR beam depends on both geometrical and optical characteristics of the beamline [11–13].

The first demonstration of FTIRM with a synchrotron IR source was in the early 1990s when a custom built IR microscope was installed at the National Synchrotron Light Source (Upton, NY) [14,15], while similar efforts were underway at UVSOR in Japan at the same time [16]. The first commercial IR microscope was installed at the NSLS a few years later [7,17]. Since then, IR microscopes have been installed on over 15 beamlines at synchrotrons worldwide, and an equal number are currently in the planning or construction stages.

3. Instrumentation

3.1. Infrared beamlines

A synchrotron is an electron storage ring that produces intense broadband light from X-rays through microwaves. Synchrotron light is emitted as relativistic electrons are accelerated along a circular trajectory [18]. Infrared beamlines worldwide collect synchrotron light from bending magnets in the electron storage ring. For bending magnet radiation, the "natural opening angle" (the total angle required to transmit 90% of the emitted light) is given by a simple formula: $\theta_v \cong 1.6\,(\rho\nu)^{-1/3}$, where ρ is the electron bend radius (in cm) and ν is the frequency of light (in cm^{-1}). As an example, the VUV-IR ring at the NSLS (Brookhaven National Laboratory) has a bending magnet radius of 1.91 m, giving a natural opening angle of 28 mrad at 10 μm, and ~62 mrad at 100 μm. The IR microscope beamlines at the NSLS are designed around an extraction system that collects ~40 mr from the storage ring — an opening angle that collects essentially all of the infrared light down to 250 cm^{-1} (λ = 40 μm), and the collection efficiency decreases slowly with frequencies below this value. As a general rule, the light collected from a bending magnet is linearly polarized in the plane of the electron beam orbit, while the off-axis radiation is elliptically polarized [12]. Engineering constraints on newer third-generation synchrotrons prohibit the large vertical opening angles required to extract long-wavelength IR photons [12]. In this case, the smaller opening angle of radiation produced at the entrance or exit edge of a bending magnet provides an advantage [19]. Today, several synchrotron IR beamlines utilize radiation from the edge of the dipole magnet, which is emitted along the straight section axis in a hollow cone [20–22]. While the emission pattern and properties of edge-radiation differ from ordinary synchrotron light (e.g., edge radiation beamlines produce radially polarized light [11,23]), these beamlines provide comparable flux and brightness [11,13,19,23].

Extraction of the synchrotron light from the storage ring is generally accomplished with a combination of gold- or aluminum-coated plane and toroid/ellipsoid or spherical mirrors (Fig. 2). The first extraction mirror must handle the heat load of higher energy photons (i.e., X-rays), so water-cooling, water-cooled masks, and/or slotted mirrors are often employed. The infrared light is focused through an infrared-transparent window (usually diamond, but in a few cases IR transparent windows such as KBr, ZnSe and KRS5 have been used), which separates the ultrahigh vacuum (UHV) conditions of the storage ring (10^{-9} to 10^{-10} Torr) and the rough vacuum of the IR beamline (10^{-3} to 10^{-4} Torr). The beam is then re-collimated and directed into the IR microscope. IR beamlines are generally terminated with an IR-transparent window (KBr, CsI, polyethylene) to isolate the beamline vacuum from the ambient pressure of the microscope. Although IR light passes easily through air, water vapor and carbon dioxide (CO_2) in the air are highly absorbing, so IR microscopes are typically purged with dry nitrogen or dry air.

3.2. Synchrotron infrared microscopes

Infrared microscopes are commercially available from a number of companies worldwide. Very little modification is needed to adapt a commercial microscope for a synchrotron infrared source. The collimated beam of synchrotron IR light

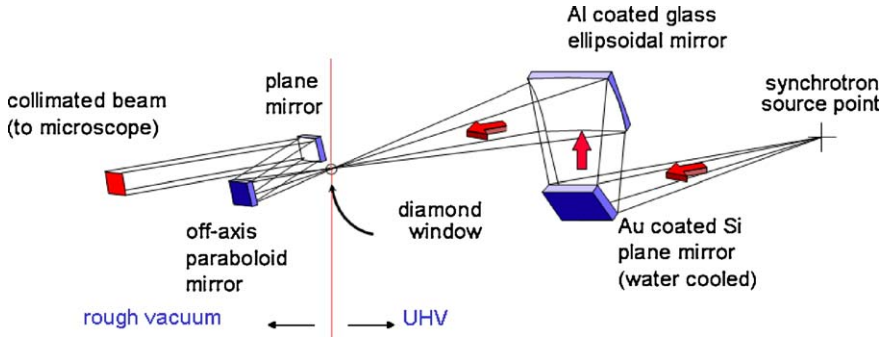

Fig. 2. Schematic of synchrotron infrared beamline extraction optics at the NSLS. All components before the diamond window are at ultra-high vacuum. Reproduced from [18].

follows the same beam path as the conventional thermal IR source. Thus in general, a simple flat mirror is used to easily switch between the thermal and synchrotron source. From the end of the beamline, the collimated beam of synchrotron IR light first enters the FTIR spectrometer and then is directed towards the IR microscope.

Infrared microscopes are very much like conventional visible light microscopes. The IR light follows the same path as the sample illumination light, so that IR microspectroscopy can be performed on the sample at the center of the viewing field. Because of their design, they are also equipped with a number of convenient methods for enhanced sample visualization. These include polarized light (visible and IR), fluorescence illumination, and differential interference contrast (DIC).

Typically, IR microscopes are configured in one of two ways —for FTIRM or FTIRI (Fig. 3). In a few cases, single IR microscopes can operate in both configurations. For an FTIRM instrument, a small area (a 'point') is spectroscopically sampled by the instrument, and an image is built-up by raster-scanning the specimen through the focused beam. Since only a single point is sampled at a time, these instruments use a single-element detector. The microscope uses reflecting Schwarzschild-type objectives to avoid absorption and chromatic aberrations over the large mid-IR spectral range. One objective serves to focus the

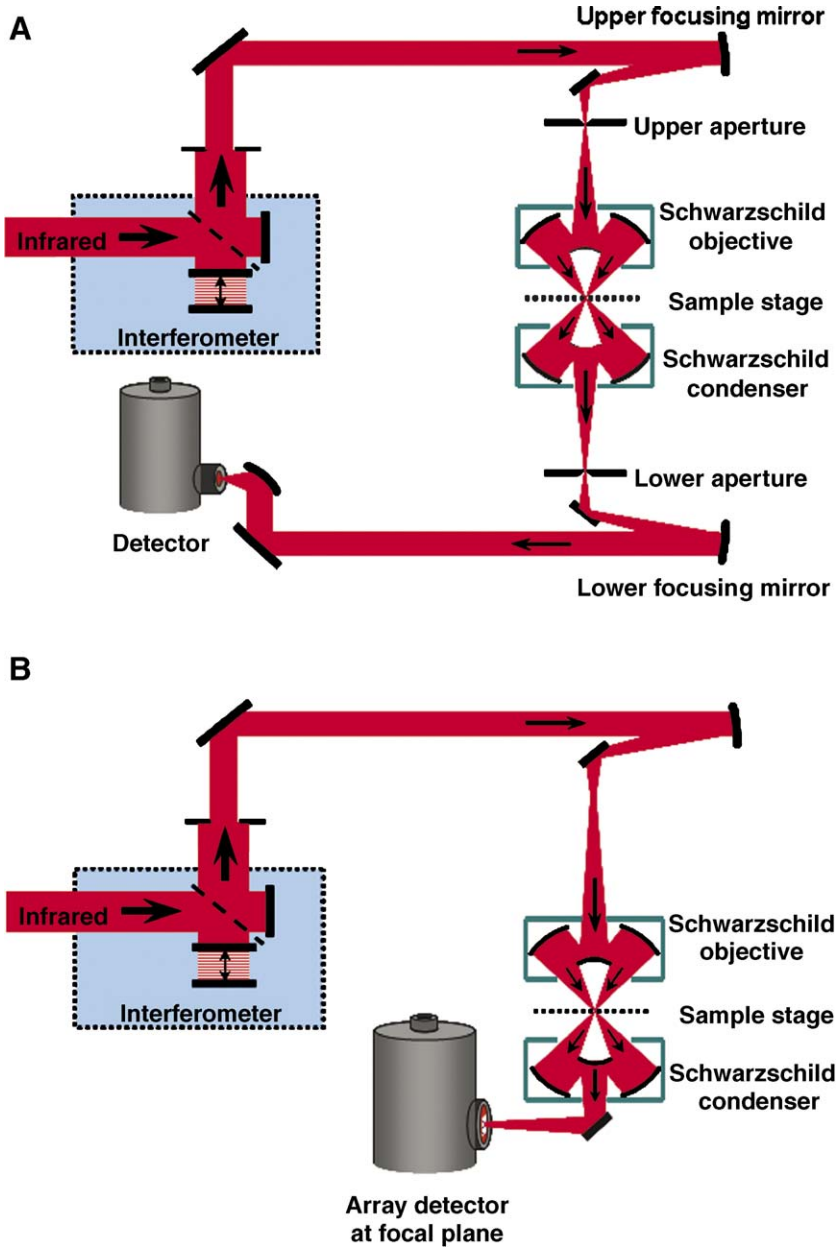

Fig. 3. (A) Schematic for a scanning IR microspectrometer system using a single-element detector and the possibility for confocal operation where aperturing is used both before and after the sample. (B) Schematic for an imaging IR microspectrometer system using an FPA detection system. Note that the 'upper' aperture must be left 'open' or removed to allow light to fall onto the entire area to be imaged. Reproduced from [13].

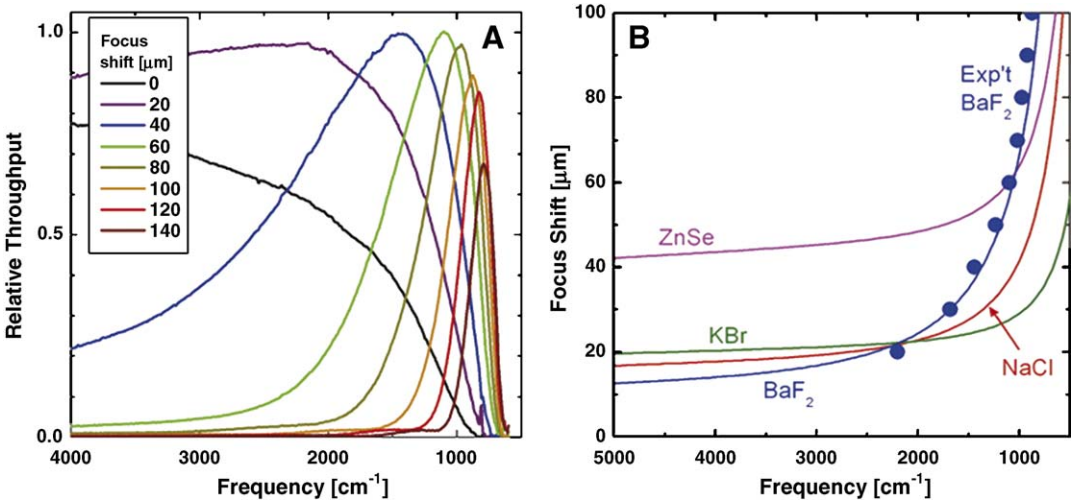

Fig. 4. (A) Relative transmission through a 2 mm thick BaF_2 substrate at various focus settings. (B) Lines: calculated focus shift for several common IR materials (all 2 mm thick) including BaF_2. Closed circles: measured focus shift for BaF_2. Reproduced from [5].

light onto the specimen, while the other collects the light and relays it on to the detector. An aperture is used to constrain the illuminated or detected area on the specimen.

In an FTIRI microscope, Schwarzschild objectives are also used, but the system is apertureless, i.e., it does not provide any spatial discrimination. Instead, the first objective illuminates a rather large area, and this illuminated region is then imaged onto the FPA detector by the second Schwarzschild objective. Spatial discrimination is provided by the individual pixels of the detector, each one serving as its own "aperture". Because there is no matching aperture for the illumination objective, this system does not operate in a confocal arrangement.

Both FTIRM and FTIRI instruments are designed with 2 paths from the sample to the detector: transmission and reflection. In transmission mode, the IR light passes through the sample and is collected by a second IR objective that re-collimates the beam and sends it to the IR detector. In reflection mode, the IR light reflects off of the sample and passes back through the illuminating objective. In this configuration, approximately 40–50% of the incident IR light is blocked by a mirror that collects the reflected light. This fraction can be reduced significantly with a synchrotron IR source, providing a large throughput advantage over the conventional thermal source in reflection mode.

3.3. Infrared detectors

Infrared microscopes are generally equipped with detectors of high responsivity, generally liquid nitrogen-cooled, broad-band or narrow-band mercury cadmium telluride (MCT). The long wavelength cutoff for this tunable alloy system is usually set to 650 cm^{-1}, which provides good compromise between spectral range and S/N. Longer wavelength MCT detectors (e.g., down to 450 cm^{-1}) are also available, their intrinsic detectivity is lower, reducing the achieved S/N by a factor of 2 to 5 compared to 650 cm^{-1} cut-off MCT detectors. One drawback of the MCT detector is its non-linear response, where the high brightness of the synchrotron source leads to highly localized intensity on the detector. Better linearity in detector response is achieved with extrinsic germanium photoconductor detectors [18]. Since a synchrotron IR source produces light well into the far-infrared region, IR microscopes are also equipped with low frequency detectors (e.g., Cu-doped Ge, B-doped Si, bolometer). These detectors are generally large in size because they are cooled by liquid helium, so they are mounted external to the IR microscope [24]. However, new developments in micro bolometric detectors have been recently reported [25].

The most recent development in IR detectors involves the coupling of an IR focal-plane array (FPA) detector to an interferometer [2,3]. To date, the size and arrangement of the individual detector elements have not been optimized for a synchrotron-powered IR microscope primarily because of their optical design and light coupling. Specifically, the FPA collects the projected image of the IR beam onto the sample, which is quite large due to the large source size of the conventional

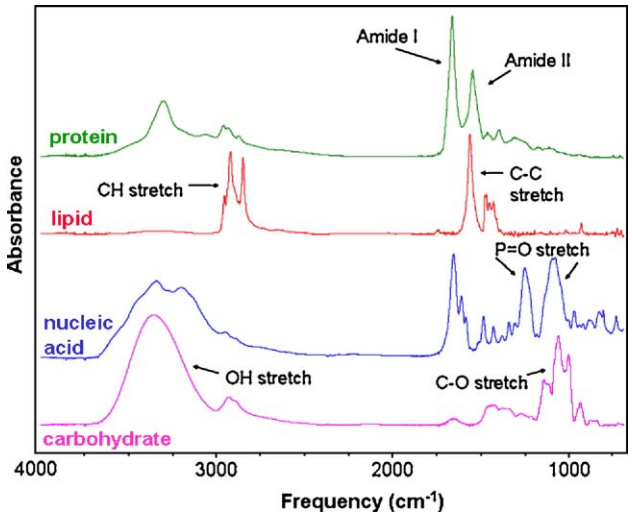

Fig. 5. IR spectra of biological components highlighting the most prominent absorption features. Spectra for a protein (myoglobin), lipid (dimyristoylphosphatidylcholine, DMPC), nucleic acid (poly-A), and carbohydrate (sucrose) are shown.

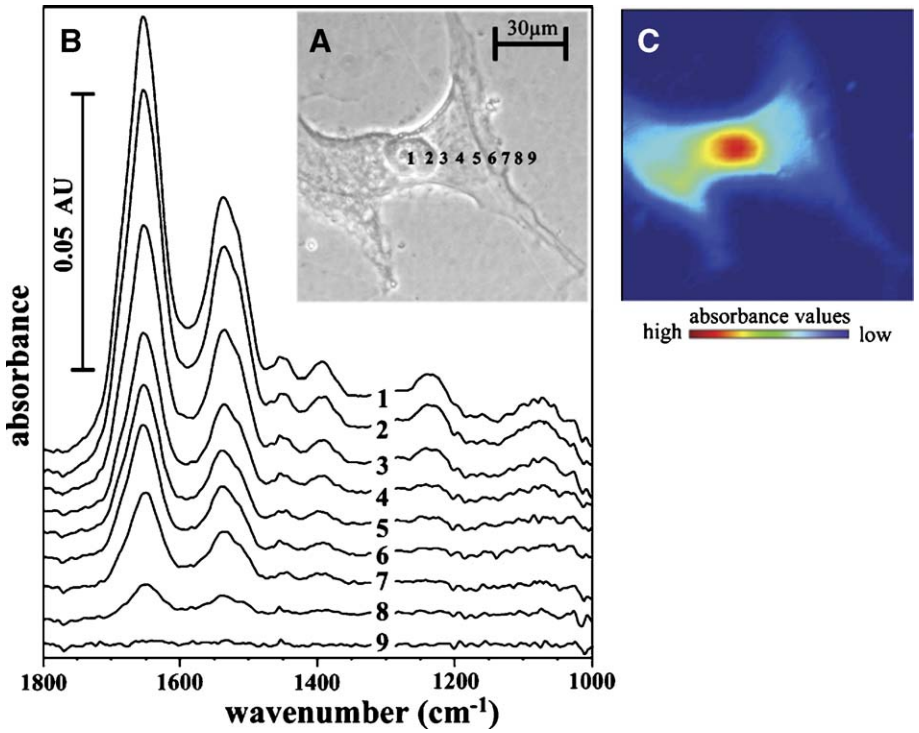

Fig. 6. Synchrotron infrared imaging of a benign human skin fibroblast showing the (A) visual image, (B) representative infrared spectra acquired along the black line in (A), and (C) protein infrared image. Cells were grown onto a CaF_2 slide, treated with ethanol and RNAse to remove phospholipids and RNA, respectively. Thus, the nucleic acid vibrations observed at ca. 1080 and 1235 cm^{-1} are due to DNA. Spectra were collected with a square aperture of 8×8 μm in transmission mode. Reproduced from [52].

globar (a few mm^2). Each FPA detector element records the spectrum of the corresponding projected pixel size onto the sample. With the small inherent source size of the synchrotron beam, the brightness advantage would be lost if the beam were expanded to accommodate the same projected size. However, early attempts using an FPA with 64×64 elements have already shown the greater advantage of using the synchrotron source (Carr, et al., in preparation; Mathis et al., private communication).

4. Sample preparation and modes of data collection

Sample preparation is perhaps the most critical part of a successful IR microspectroscopy experiment. Since there are a number of ways to use the IR microscope to collect spectra, sample preparation can also be done in a variety of ways. Since biological materials are most frequently probed in transmission- or reflection-mode, these methods will be described here. Other methods are also available, such as grazing incidence and attenuated total reflection (ATR) [1].

4.1. Transmission

Perhaps, the preferred way to collect IR microspectra is in transmission mode. In this mode, thin samples are needed. Although it is very sample-dependent, typical thicknesses for transmission measurements are 5–30 μm. Polymers, unmineralized biological tissues, and other organic materials are generally prepared with thicknesses of 10–15 μm. Minerals (biological and geological) are much more variable, depending on the specific material. Fully mineralized bone is typically sectioned at 3–5 μm.

The method of choice for preparing thin sections of biological tissue is cryogenic sectioning with a microtome. This method best preserves the original state of the tissue and does not involve embedding materials. However, cryo-sectioning is often not possible. In these cases, thin samples are often prepared by embedding the sample in a matrix and then cutting with a microtome. Embedding compounds are generally chosen to match the hardness of the sample. For mineralized tissues and other hard materials, a variety of polymers are available [26]. For soft tissues, paraffin is often used. However, care must be taken to choose an embedding process that does not affect the chemistry of the sample. Also, since these compounds usually penetrate throughout the sample, a material should be chosen that does not have IR absorption features that overlap those of the sample. For example, paraffin is often used to embed unmineralized biological tissues because its most intense absorbance features are limited to the C–H stretch region (2800–3000 cm^{-1}). However, weaker C–C stretching modes fall near 1465 cm^{-1}, which can also interfere with the sample spectrum. Moreover, the process of paraffin-embedding requires sample dehydration and fixation, which can alter the chemistry of the sample to be probed. Thus, the sample component(s) of interest must be robust enough to handle this process.

Once a thin section is cut, it is placed on an infrared-transparent material with thickness ranging from nanometers to millimeters. For biological materials, transparent, water-insoluble substrates such as CaF_2 and BaF_2 are most common. When

using IR-transparent substrates and working with the small spot sizes of a synchrotron IR source, the effect of dispersion must be considered during data collection [5]. Specifically, most of the IR-transparent materials have some degree of dispersion in the visible, infrared, or both. For typical thicknesses of these materials (1–2 mm), this dispersion leads to focusing errors of 20 μm or more, and severe loss of signal or spatial resolution occurs over part, or all, of the spectral range of interest. In order to compensate for substrate dispersion, defocusing of the collection optics (i.e., condenser) is critical (Fig. 4).

4.2. Reflection

Another way of collecting IR microspectra is in reflection mode. Samples probed in reflection mode are most often (1) highly reflective or polished samples that cannot be cut to thin sections, or (2) microtomed thin sections that are placed on an IR-reflective substrate instead of an IR-transparent substrate. Recently, reflection mode has become more popular for probing microtomed thin sections that have been placed on IR-reflective substrates. For these experiments, the IR beam penetrates through the sample, reflects off the substrate, and then passes back through the sample again. Since the beam passes through the sample twice, the result is a "double-absorption" spectrum. For this reason, the thin sections should be cut to ~1/2 the thickness used for a transmission measurement.

Semi-reflective and polished samples are also probed in reflection mode. Since the S/N of the spectra relies strongly on collection of the reflected light back into the IR objective, it is important that these samples have a smooth, flat surface and correctly oriented. Samples that have smooth surfaces that are not flat can be mounted into a micro-goiniometer to adjust the tilt of the sample with respect to the incoming beam. Even simpler, samples can also be pressed into a small sphere of putty so that the sample surface is parallel to the microscope stage.

While thin sections are often easier to prepare on IR-reflective substrates, the use of IR-reflective substrates does come at a cost to the IR data collection process and even spectral quality. As noted earlier, the incident flux in reflection mode is reduced by almost 50% compared to transmission mode, since only half of the focusing objective is used to direct the beam onto the sample, and the second half is used for collecting the reflected beam. In addition, any inhomogeneities in the thin section can cause interference effects (e.g., oscillations) in the background of the IR spectra. These artifacts can alter peak shapes, intensities, and frequencies. Thus, care must be taken with sample preparation, and only certain (generally homogeneous) samples work well in this mode.

5. Biological and medical applications of synchrotron IR microspectroscopy

Infrared microspectroscopy has been used to examine numerous plant and animal tissues, even before the union of the IR microscope and the synchrotron source [27]. For complex samples such as human tissues, an infrared spectrum provides a direct indication of sample biochemistry. Fig. 5 illustrates IR spectra of a common phospholipid (DMPC, dimyristoylphosphatidycholine), protein (myoglobin), nucleic acid (poly-A), and carbohydrate (sucrose). The dominant absorption features in the lipid spectrum are found in the region 2800–3000 cm^{-1}, and are assigned to asymmetric and symmetric C–H stretching vibrations of CH_3 (2956 and 2874 cm^{-1}) and CH_2 (2922 and 2852 cm^{-1}). In addition, the strong band at 1736 cm^{-1} arises from ester C═O groups in the lipid. The protein spectrum has two primary features, the Amide I (1600–1700 cm^{-1}) and Amide II (1500–1560 cm^{-1}) bands, which arise primarily from the C═0 and C–N stretching vibrations of the peptide backbone, respectively. The frequency of the Amide I band is particularly sensitive to protein secondary structure

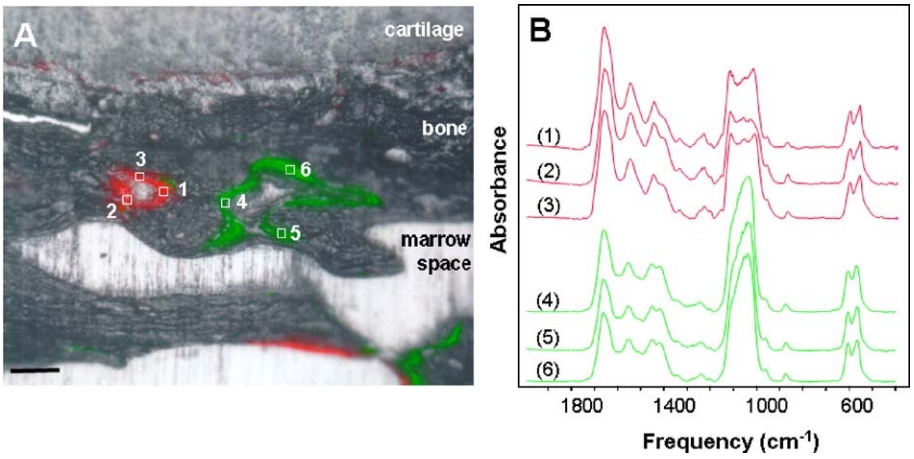

Fig. 7. (A) Epifluorescence microscopy image of fluorochrome-labeled regions of osteoporotic monkey bone. Calcein (green) indicates bone deposited 1 year after ovariectomy. Xylenol orange (red) indicates bone deposited 2 years after ovariectomy. Newly remodeled bone is deposited in layers 3–5 μm thick, and thus can only be probed with a synchrotron IR source. (B) S-IR microspectra collected from calcein- and xylenol-labeled bone. Results showed that bone deposited 2 years after ovariectomy was less mineralized than bone deposited at 1 year, suggesting that the mineralization rate of osteoporotic bone was reduced. Aperture size was 10 μm. Adapted from [84].

[28,29]. In the nucleic acid spectrum, the region between 1000 and 1500 cm^{-1} contains contributions from asymmetric (1224 cm^{-1}) and symmetric (1087 cm^{-1}) PO_2^- stretching vibrations.

The assignments of various spectral features in biological samples have been the subject of numerous publications, which have been reviewed recently [30]. Armed with information on sample histology and pathology, variations in nucleic acid, protein, and lipid content or structure, can provide important details about the chemistry of diseased states. With the high spatial resolution of the synchrotron, individual cells within a tissue can be probed with sub-cellular resolution. For example, the structure of misfolded protein aggregates has been identified in the brain tissue of Alzheimer's disease patients [31–33] and infectious prion proteins have been characterized in scrapie [34–37]. Variations in bone composition have been observed in osteoporosis [38,39], osteopetrosis [40], and osteoarthritis [41]. In heart disease, altered lipid and collagen content and structure in the myocardium have been seen [42], which were partially normalized by losartan treatment [43].

The high spatial resolution of a synchrotron IR source permits the subcellular chemical mapping of single living cells for the first time (Fig. 6). Sample heating has been shown to be negligible, permitting analysis of single cells for time scales from hours to days [44,45]. Individual mouse hybridoma B cells have been examined during necrosis and the end phases of mitosis [46], and also during the process of apoptosis [47]. Metal-cyanobacteria sorption reactions have been characterized in detail[48]. Spectral differences have been seen between normal and cancerous oral epithelial cells [49–52], healthy and nutrient-repleted Micrasterias hardyi algal cells [53], and HepG2 cells exposed to low doses of 2,3,7,8-tetrachlorodibenzo-p-dioxin [54]. Variations in DNA/RNA content and packing have also been demonstrated during the cell cycle of human lung epithelial cells [55].

FTIRM has recently been combined simultaneously with epifluorescence microscopy [56,57] to probe 5 μm-wide layers of newly deposited bone [38,39,58], plaques in Alzheimer's disease [32], and different stages of apoptosis [47]. Fig. 7 illustrates how epifluorescence microscopy was used to visualize fluorochrome labels in osteoporotic bone while synchrotron FTIRM was used simultaneously to assess mineralization levels. Other visualization techniques include the use of polarized light and differential interference contrast (DIC). On the cellular and sub-cellular level, these techniques can be used to visualize fluorescent tags bound to particular cellular components and even antibodies to individual proteins. Once identified, the IR microscope can be used to analyze the chemical environment in and around that region of interest. It should be noted that fluorescent labels are generally present in extremely low (i.e., nanomolar) concentrations, so they do not interfere with the IR technique; they are used exclusively for visualizing a region of interest.

A considerable amount of analysis has been done recently on the chemical composition of human hair. For hair, the synchrotron IR source provides the ability to probe the cuticle (~5 μm width), cortex (~40–80 μm width), and medulla (~10 μm width) substructures separately (Fig. 8) [59,60]. Lipid concentrations have been found to be elevated in the medulla, whereas variations in protein structure exist among the different regions [59,61]. Bleaching of hair affects the hydration level of the cuticle, and also causes the formation of sulfonate (S═O) groups in the cortex [62]. Keratin disorganization has been observed in hair of ancient Egyptian mummies, likely due to peptide bond breakage [63], and narcotics in human hair have also been observed [64].

Since infrared spectroscopy probes the vibrational frequency of a bond, elemental isotopes can be used as targets to study biochemical processes. For example, the transport of D_2O from the gut to the brain was studied in adult rats [65]. Results showed that the CD:CH and ND,OD:NH,OH ratios were highest in the molecular layer of the brain and lowest in the white matter. The high ratios in the molecular layer are consistent with the active synthesis and recycling at synapses, which are abundant structures in this layer. The low levels in the white matter are consistent with radioactive measures that found slow turnovers of proteins and lipids in myelin, which is the main constituent of white matter.

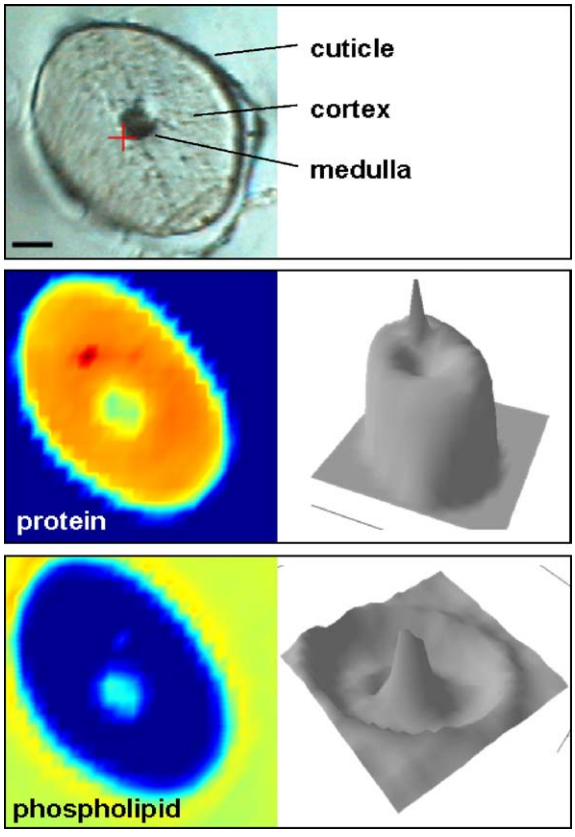

Fig. 8. Synchrotron infrared images of the cross-section of a human hair. Hair contains three substructures that can only be resolved with the high spatial resolution of a synchrotron IR source. From the center outward, these substructures and their thicknesses are: medulla (10–20 μm), cortex (30–100 μm) and cuticle (2–5 μm). IR imaging of these regions show that the protein concentration (1700–1600 cm^{-1}) is highest in the cortex, while phospholipid (1750–1700 cm^{-1}) concentration is highest in the medulla and cuticle. Scale bar is 25 μm.

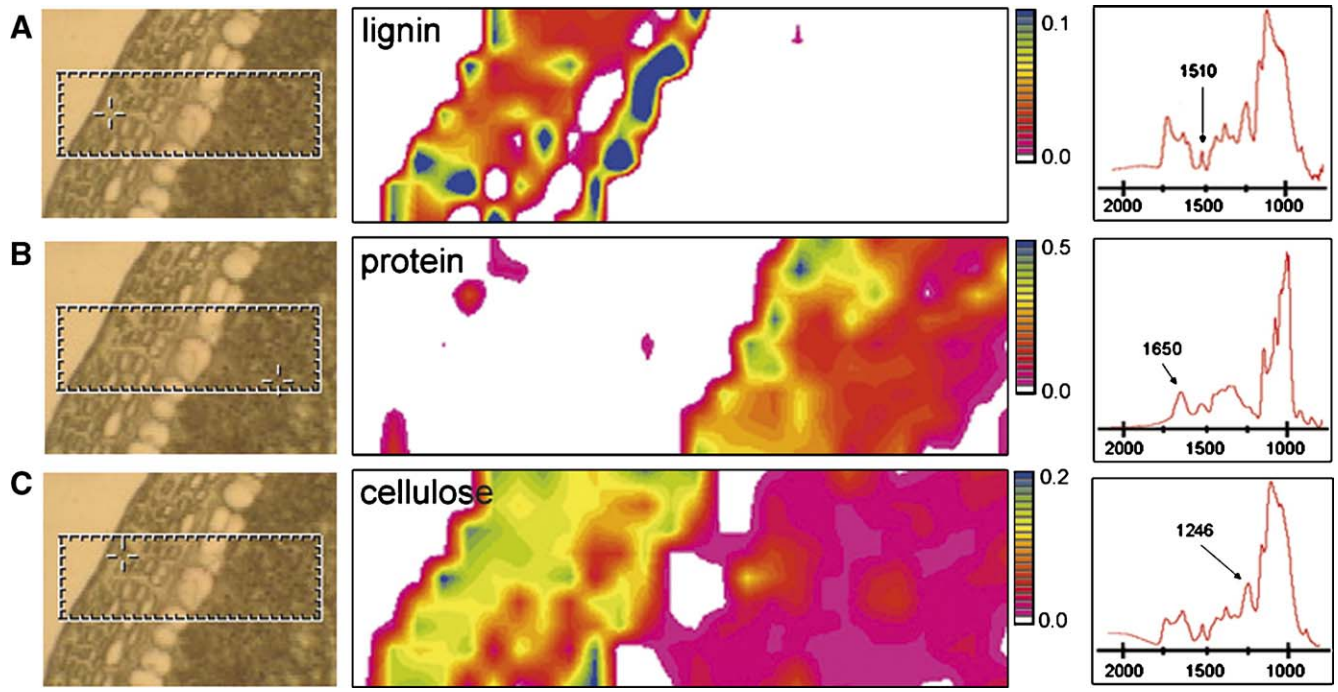

Fig. 9. Synchrotron FTIRM imaging of Pioneer corn showing the distribution of (A) lignin (1510 cm^{-1}), (B) protein (1650 cm^{-1}) and (C) cellulose (1246 cm^{-1}). Results show varying concentrations of these components in the pericarp, seed coat, aleurone, and endosperm. The area imaged with the IR microscope was 250 μm (horizontal) ×80 μm (vertical) with a square aperture size of 10 μm. Adapted from [67].

In addition to animal tissue and cells, synchrotron FTIRM has been used to characterize plant composition as well. Fewer studies have been done, likely hampered by difficulties in preparing thin sections of fragile plant roots, stems, and leaves. Regardless, the distribution of plant components such as lignin, cellulose and other carbohydrates, proteins, and lipids reveals specific information on the biochemistry of the plant (Fig. 9) [66–68]. For example, the starch content and relative fraction of α-helical protein structure has been characterized in hard versus soft wheat [69] and two types of winterfat (forage) seeds [70], the transport of organic contaminants has been observed [71], and chemical differences and similarities within the root zone of mung bean (*Vigna radiata* L.), grown with or without phosphorus, have been characterized [72].

Synchrotron FTIRM has also been used in less-traditional ways to study biological systems. For example, in a recent study a synchrotron IR microscope was coupled to a rapid-mix flow cell in order to study protein folding on a microsecond time scale. The small spot size of the synchrotron beam permitted higher spatial resolution of the technique, and the use of smaller volumes of sample [73,74].

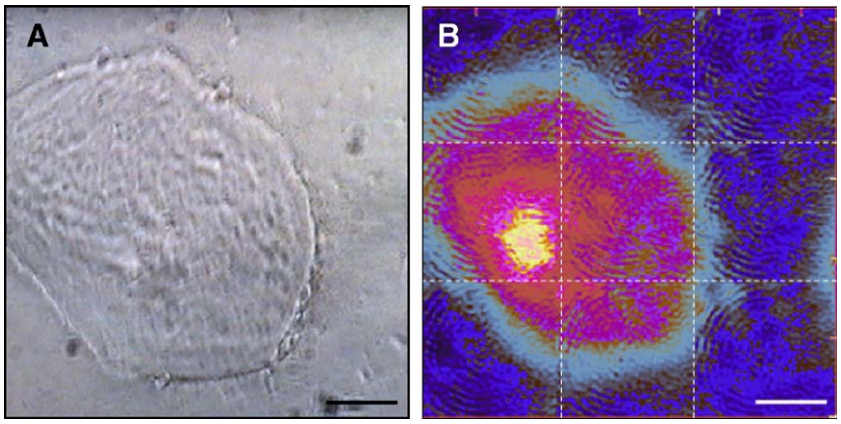

Fig. 10. (A) Bright field visible image of a human oral mucosa cell. (B) Synchrotron FPA image of the protein (Amide I) absorbance in the oral mucosa cell. The sample was illuminated with a low magnification objective (36X, 0.6 NA) for long working distance and collected with a high magnification (74X, 0.6 NA) objective. A 64 × 64 pixel MCT FPA detector was used to image the cell, where the resulting field of view on the FPA was 35 × 35 μm with 0.54 μm per pixel. The IR image (192 × 192 pixels) was generated in 72 min with a 64 × 64 pixel FPA detector (200 scans, 6 cm^{-1} resolution). Scale bar is 20 μm.

Another recent example of a non-traditional experiment involved the use a of pump-probe technique to study the influence of an optically thick applied water layer on the laser ablation of tooth enamel [75]. Laser ablation was performed in the presence and absence of water, and synchrotron FTIRM was used to probe the chemical composition of the enamel in the formed crater. Results revealed the formation of new mineral phases deposited along the crater walls after repetitive laser pulses and such non-apatitic phases reduce the efficiency of ablation. The application of a water layer removes such loosely adherent phases, maintaining efficient ablation during multiple-pulse irradiation.

6. Future directions for synchrotron infrared microspectroscopy

To date, the vast majority of synchrotron FTIRM experiments have been performed on static systems, at ambient pressure and temperature, and in the mid-infrared spectral region. There have been a few exceptions, some of which were described above.

Future FTIRM experiments promise to include time-resolved measurements, from long time scales (minutes to hours) to time scales that take advantage of the pulsed structure of the synchrotron beam (10 s to 100 s of picoseconds). Though the pulse duration is significantly longer than what can be achieved with ultra-fast lasers (10 s to 100 s of femtoseconds), the synchrotron is a "white" source that allows complete spectral information to be acquired. This provides a unique opportunity to study dynamics associated with chemical bonds. It is possible that future generations of synchrotron light sources will produce pulses with durations of ~100 fs or less.

Other areas of growth include applications to systems studied over wide temperature and pressure ranges, and spectra taken over a much broader spectral range, including far-infrared or terahertz (THz or T-Ray) FTIRM. Many infrared studies have shown that protein and lipid membrane structures are sensitive to temperature and pressure, yet none have involved spatially-resolved IR imaging [76–79]. Both proteins and nucleic acids have also been studied in the far-infrared regime [80,81], but none have taken advantage of the high spatial resolution of a synchrotron IR microscope. On the other end of the spectrum, combined X-ray (fluorescence or absorption) and IR microscopic analyses on the same sample represents an activity of growing interest in the biomedical community [32,37,82,83]. The throughput limits of cryogenic and/or high-pressure microspectroscopy and brightness limits of X-ray/far-infrared microspectroscopy represent a particular challenge that only a synchrotron source can fulfill.

Finally, while current synchrotron FTIRM measurements provide the highest possible spatial resolution, they are time-consuming because they utilize a confocal arrangement with a single-element IR detector. Raster-scanned images of a single biological cell can take more than an hour to collect, and subcellular imaging of significant regions of tissue can take several days. To date, a comprehensive FTIRI study with a FPA detector has not been performed on with a synchrotron source, but the rapid speed at which FPA detectors collect data make them an appealing alternative for some chemical imaging measurements.

When imaging biological systems at the diffraction limit, a confocal optical arrangement can improve the spatial resolution and image contrast. But this optical configuration is inherently incompatible with FPA detection systems having contiguous pixels. However, having an accurate knowledge of the diffraction pattern implies that a mathematical correction for diffraction is possible by deconvolution methods. But for acceptable results, deconvolution requires both high spatial oversampling and excellent S/N. It is likely that these requirements may not be achievable with a conventional thermal source. For example, high resolution sampling can be accomplished using an FPA and a high magnification objective, but the flux incident on each pixel may be more than 100× smaller such that the S/N is not sufficient for a successful deconvolution [13]. The synchrotron source has the potential to correct for diffraction effects and improve the spatial resolution of FTIRI over regions of modest size (Fig. 10). Thus, we expect that the synchrotron and thermal sources are likely to play complementary roles. The thermal source is capable of illuminating large regions and is well suited to surveying large areas. The synchrotron has its intensity concentrated in a small area, and is typically used for microsampling (i.e., collecting spectra from small objects with minimal contamination from neighboring regions) or to produce high spatial resolution images of small areas — typically smaller than 100 μm on a side. We anticipate a similar role for the FPA detector, with the thermal source surveying areas many millimeters on a side and offering excellent performance down to about 10 μm spatial resolution. With the synchrotron, we anticipate that the resolution limit may be extended down to around 1 μm, but over a much more limited area.

7. Synchrotron IR facilities worldwide

Facilities for IR synchrotron radiation can be found throughout the world, serving to produce light for the scientific community. In North America, the National Synchrotron Light Source (Upton, NY) presently operates six IR beamlines, with four IR microscopes. Active IR microspectroscopy beamlines can also be found at the CLS (Saskatoon, SK), ALS (Berkeley, CA), SRC (Stoughton, WI), and CAMD (Baton Rouge, LA). In Asia, IR programs exist at UVSOR (Osaka, Japan), SPring8 (Nishi-Harima, Japan), and NSRRC (Hsinchu, Taiwan). In Europe, IR activities continue at the SRS (Daresbury, UK), ESRF (Grenoble, France), MAXLAB (Lund, Sweden), Daφne (Frascati, Italy), Elettra (Trieste, Italy), ANKA (Karlsruhe, Germany), and BESSY II (Berlin, Germany). Other facilities that are planning IR microspectroscopy programs include Diamond (Rutherford Lab, UK); SOLEIL (Paris, France), DELTA (Dortmund, Germany), SLS (Villigen, Switzerland), the Australian Synchrotron (Melbourne, Australia), NSRL (Hefei, China), SSRL (Singapore), and Pohang (Korea).

Acknowledgements

The authors would like to acknowledge Larry Carr, Gwyn Williams, and Randy Smith for data contributions and many valuable discussions. LMM is partially supported by the National Institutes of Health (GM66873). The NSLS is

supported by the United States Department of Energy under contract DE-AC02-98CH10886.

References

[1] H. Humecki, Practical Applications of Infrared Microspectroscopy, Marcel Dekker, Inc., New York, 1995.
[2] E.N. Lewis, P.J. Treado, R.C. Reeder, G.M. Story, A.E. Dowrey, C. Marcott, I.W. Levin, Fourier-transform spectroscopic imaging using an infrared focal-plane array detector, Anal. Chem. 67 (1995) 3377–3381.
[3] S.W. Huffman, R. Bhargava, I.W. Levin, Generalized implementation of rapid-scan Fourier transform infrared spectroscopic imaging, Appl. Spectrosc. 56 (2002) 965–969.
[4] R.G. Messerschmidt, in: H. Humecki (Ed.), Practical Guide to Infrared Microspectroscopy, Marcel Dekker, Inc., New York, 1995, pp. 3–40.
[5] G.L. Carr, Resolution limits for infrared microspectroscopy explored with synchrotron radiation, Rev. Sci. Instrum. 72 (2001) 1613–1619.
[6] W. Duncan, G.P. Williams, Appl. Opt. 22 (1983) 2914.
[7] G.L. Carr, J.A. Reffner, G.P. Williams, Performance of an infrared microspectrometer at the NSLS, Rev. Sci. Instrum. 66 (1995) 1490–1492.
[8] J.A. Reffner, P.A. Martoglio, G.P. Williams, Fourier transform infrared microscopical analysis with synchrotron radiation: the microscope optics and system performance, Rev. Sci. Instrum. 66 (1995) 1298.
[9] L.M. Miller, R.J. Smith, Synchrotrons versus globars, point-detectors versus focal plane arrays: selecting the best source and detector for specific infrared microspectroscopy and imaging applications, Vib. Spectrosc. 38 (2005) 237–240.
[10] G.L. Carr, High-resolution microspectroscopy and sub-nanosecond time-resolved spectroscopy with the synchrotron infrared source, Vib. Spectrosc. 19 (1999) 53–60.
[11] R.A. Bosch, Focusing infrared edge and synchrotron radiation with a large numerical aperture, Nucl. Instrum. Methods Phys. Res., Sect. A, Accel. Spectrom. Detect. Assoc. Equip. 492 (2002) 284–298.
[12] A. Nucara, S. Lupi, P. Calvani, The infrared synchrotron radiation beamline at the third generation light source ELETTRA, Rev. Sci. Instrum. 74 (2003) 3934–3942.
[13] G.L. Carr, O. Chubar, P. Dumas, in: R. Bhargava, I.W. Levin (Eds.), Spectrochemical Analysis Using Infrared Detectors, Blackwell Publishing, 2006, pp. 56–84.
[14] G.P. Williams, Infrared synchrotron radiation instrumentation and applications, Rev. Sci. Instrum. 63 (1992) 1535.
[15] M. Hanfland, R.J. Hemley, H.K. Mao, G.P. Williams, Synchrotron infrared-spectroscopy at megabar pressures — vibrational dynamics of hydrogen to 180 Gpa, Phys. Rev. Lett. 69 (1992) 1129–1132.
[16] A. Ugawa, H. Ishii, K. Yakushi, H. Okamoto, T. Mitani, M. Watanabe, K. Sakai, K. Suzui, S. Kato, Design of an instrument for far-infrared microspectroscopy using a synchrotron radiation source, Rev. Sci. Instrum. 63 (1992) 1551–1554.
[17] G.L. Carr, M. Hanfland, G.P. Williams, Mid-infrared beamline at the national synchrotron light source port U2B, Rev. Sci. Instrum. 66 (1995) 1643–1645.
[18] G.L. Carr, G.P. Williams, Infrared microspectroscopy with synchrotron radiation, SPIE Conf. Proc. 3153 (1997) 51–59.
[19] R.A. Bosch, Computed flux and brightness of infrared edge and synchrotron radiation, Nucl. Instrum. Methods Phys. Res., Sect. A, Accel. Spectrom. Detect. Assoc. Equip. 454 (2000) 497–505.
[20] U. Schade, A. Roseler, E.H. Korte, M. Scheer, W.B. Peatman, Measured characteristics of infrared edge radiation from BESSY II, Nucl. Instrum. Methods Phys. Res., Sect. A, Accel. Spectrom. Detect. Assoc. Equip. 455 (2000) 476–486.
[21] R.A. Bosch, Extraction of edge radiation within a straight section of Aladdin, Rev. Sci. Instrum. 73 (2002) 1423–1426.
[22] Y.L. Mathis, B. Gasharova, D. Moss, Terahertz radiation at ANKA, the new synchrotron light source in Karlsruhe, J. Biol. Phys. 29 (2003) 313–318.
[23] R.A. Bosch, Focusing of infrared edge and synchrotron radiation, Nucl. Instrum. Methods Phys. Res., Sect. A, Accel. Spectrom. Detect. Assoc. Equip. 431 (1999) 320–333.
[24] L.M. Miller, G.D. Smith, G.L. Carr, Synchrotron-based biological microspectroscopy: From the mid-infrared through the far-infrared regimes, J. Biol. Phys. 29 (2003) 219–230.
[25] A.J. Kreisler, A. Gaugue, Recent progress in high-temperature superconductor bolometric detectors: from the mid-infrared to the far-infrared (THz) range, Supercond. Sci. Technol. 13 (2000) 1235–1245.
[26] S. Aparicio, S.B. Doty, N.P. Camacho, E.P. Paschalis, L. Spevak, R. Mendelsohn, A.L. Boskey, Optimal methods for processing mineralized tissues for Fourier transform infrared microspectroscopy, Calcif. Tissue Int. 70 (2002) 422–429.
[27] D.L. Wetzel, S.M. LeVine, Imaging molecular chemistry with infrared microscopy, Science 285 (1999) 1224–1225.
[28] H. Susi, D.M. Byler, Protein structure by Fourier transform infrared spectroscopy: second derivative spectra, Biochem. Biophys. Res. Commun. 115 (1983) 391–397.
[29] D.M. Byler, H. Susi, Examination of the secondary structure of proteins by deconvolved FTIR spectra, Biopolymers 25 (1986) 469–487.
[30] M. Jackson, H.H. Mantsch, Encycl. Anal. Chem., Wiley and Sons, Chichester, 2000.
[31] L.P. Choo, D.L. Wetzel, W.C. Halliday, M. Jackson, S.M. LeVine, H.H. Mantsch, In situ characterization of beta-amyloid in Alzheimer's diseased tissue by synchrotron Fourier transform infrared microspectroscopy, Biophys. J. 71 (1996) 1672–1679.
[32] L.M. Miller, Q. Wang, T.P. Telivala, R.J. Smith, A. Lanzirotti, J. Miklossy, Synchrotron-based infrared and X-ray imaging shows focalized accumulation of Cu and Zn co-localized with beta-amyloid deposits in Alzheimer's disease, J. Struct. Biol. (2006) (in press).
[33] M. Gallant, M. Rak, A. Szeghalmi, M.R. Del Bigio, D. Westaway, J. Yang, R. Julian, K.M. Gough, Focally elevated creatine detected in amyloid precursor protein (APP) transgenic mice and Alzheimer disease brain tissue, J. Biol. Chem. 281 (2006) 5–8.
[34] J. Kneipp, P. Lasch, E. Baldauf, M. Beekes, D. Naumann, Detection of pathological molecular alterations in scrapie-infected hamster brain by Fourier transform infrared (FT-IR) spectroscopy, Biochim. Biophys. Acta 1501 (2000) 189–199.
[35] J. Kneipp, L.M. Miller, M. Joncic, M. Kittel, P. Lasch, M. Beekes, D. Naumann, In situ identification of protein structural changes in prion-infected tissue, Biochim. Biophys. Acta 1639 (2003) 152–158.
[36] J. Kneipp, L.M. Miller, S. Spassov, F. Sokolowski, P. Lasch, M. Beekes, D. Naumann, Scrapie-infected cells, isolated prions, and recombinant prion protein: a comparative study, Biopolymers 74 (2004) 163–167.
[37] Q. Wang, A. Kretlow, M. Beekes, D. Naumann, L. Miller, In situ characterization of prion protein structure and metal accumulation in scrapie-infected cells by synchrotron infrared and X-ray imaging, Vib. Spectrosc. 38 (2005) 61–69.
[38] R.Y. Huang, L.M. Miller, C.S. Carlson, M.R. Chance, Characterization of bone mineral composition in the proximal tibia of cynomolgus monkeys: effect of ovariectomy and nandrolone decanoate treatment, Bone 30 (2002) 492–497.
[39] R.Y. Huang, L.M. Miller, C.S. Carlson, M.R. Chance, In situ chemistry of osteoporosis revealed by synchrotron infrared microspectroscopy, Bone 33 (2003) 514–521.
[40] L.M. Miller, V. Vairavamurthy, M.R. Chance, R. Mendelsohn, E.P. Paschalis, F. Betts, A.L. Boskey, In situ analysis of mineral content and crystallinity in bone using infrared micro-spectroscopy of the nu(4) PO(4) (3-) vibration, Biochim. Biophys. Acta 1527 (2001) 11–19.
[41] L.M. Miller, J.T. Novatt, D. Hamerman, C.S. Carlson, Alterations in mineral composition observed in osteoarthritic joints of cynomolgus monkeys, Bone 35 (2004) 498–506.
[42] Q. Wang, W. Sanad, A. Voigt, K. Klingel, R. Kandolf, K. Stangl, G. Baumann, L.M. Miller, Infrared imaging of compositional changes in inflammatory cardiomyopathy, Vib. Spectrosc. 38 (2005) 217–222.
[43] K.M. Gough, D. Zelinski, R. Wiens, M. Rak, I.M.C. Dixon, Fourier transform infrared evaluation of microscopic scarring in the cardiomyopathic heart: Effect of chronic AT(1) suppression, Anal. Biochem. 316 (2003) 232–242.

[44] H.Y.N. Holman, M.C. Martin, W.R. McKinney, Synchrotron-based FTIR spectromicroscopy: Cytotoxicity and heating considerations, J. Biol. Phys. 29 (2003) 275–286.
[45] M.C. Martin, N.M. Tsvetkova, J.H. Crowe, W.R. McKinney, Negligible sample heating from synchrotron infrared beam, Appl. Spectrosc. 55 (2001) 111–113.
[46] N. Jamin, P. Dumas, J. Moncuit, W.H. Fridman, J.L. Teillaud, G.L. Carr, G. P. Williams, Highly resolved chemical imaging of living cells by using synchrotron infrared microspectrometry, Proc. Natl. Acad. Sci. U. S. A. 95 (1998) 4837–4840.
[47] N. Jamin, L. Miller, J. Moncuit, W.H. Fridman, P. Dumas, J.L. Teillaud, Chemical heterogeneity in cell death: combined synchrotron IR and fluorescence microscopy studies of single apoptotic and necrotic cells, Biopolymers 72 (2003) 366–373.
[48] N. Yee, L.G. Benning, V.R. Phoenix, F.G. Ferris, Characterization of metal-cyanobacteria sorption reactions: a combined macroscopic and infrared spectroscopic investigation, Environ. Sci. Technol. 38 (2004) 775–782.
[49] M.J. Tobin, M.A. Chesters, J.M. Chalmers, F.J.M. Rutten, S.E. Fisher, I.M. Symonds, A. Hitchcock, R. Allibone, S. Dias-Gunasekara, Infrared microscopy of epithelial cancer cells in whole tissues and in tissue culture, using synchrotron radiation, Faraday Discuss. 126 (2004) 27–39.
[50] P. Lasch, M. Boese, A. Pacifico, M. Diem, FT-IR spectroscopic investigations of single cells on the subcellular level, Vib. Spectrosc. 28 (2002) 147–157.
[51] M. Diem, L. Chiriboga, P. Lasch, A. Pacifico, IR spectra and IR spectral maps of individual normal and cancerous cells, Biopolymers 67 (2002) 4–5.
[52] M. Diem, M. Romeo, C. Matthaus, M. Miljkovic, L. Miller, P. Lasch, Comparison of Fourier transform infrared (FTIR) spectra of individual cells acquired using synchrotron and conventional sources, Infrared Phys. Technol. 45 (2004) 331–338.
[53] P. Heraud, B.R. Wood, M.J. Tobin, J. Beardall, D. McNaughton, Mapping of nutrient-induced biochemical changes in living algal cells using synchrotron infrared microspectroscopy, FEMS Microbiol. Lett. 249 (2005) 219–225.
[54] H.Y.N. Holman, R. Goth-Goldstein, M.C. Martin, M.L. Russell, W.R. McKinney, Low-dose responses to 2,3,7,8-tetrachlorodibenzo-p-dioxin in single living human cells measured by synchrotron infrared spectromicroscopy, Environ. Sci. Technol. 34 (2000) 2513–2517.
[55] H.N. Holman, M.C. Martin, E.A. Blakely, K. Bjornstad, W.R. McKinney, IR spectroscopic characteristics of cell cycle and cell death probed by synchrotron radiation based fourier transform IR spectromicroscopy, Biopolymers 57 (2000) 329–335.
[56] T. Tague, L.M. Miller, Novel use of fluorescence illumination with an infrared microscope, Microsc. Today 2 (2000).
[57] L.M. Miller, P. Dumas, N. Jamin, J.L. Teillaud, J. Miklossy, L. Forro, Combining IR spectroscopy with fluorescence imaging in a single microscope: biomedical applications using a synchrotron infrared source (invited), Rev. Sci. Instrum. 73 (2002) 1357–1360.
[58] B. Busa, L.M. Miller, C.T. Rubin, Y.X. Qin, S. Judex, Rapid establishment of chemical and mechanical properties during lamellar bone formation, Calcif. Tissue Int. 77 (2005) 386–394.
[59] P. Dumas, L. Miller, The use of synchrotron infrared microspectroscopy in biological and biomedical investigations, Vib. Spectrosc. 32 (2003) 3–21.
[60] K.L. Chan, S.G. Kazarian, A. Mavraki, D.R. Williams, Fourier transform infrared imaging of human hair with a high spatial resolution without the use of a synchrotron, Appl. Spectrosc. 59 (2005) 149–155.
[61] F. Briki, B. Busson, L. Kreplak, P. Dumas, J. Doucet, Exploring a biological tissue from atomic to macroscopic scale using synchrotron radiation: example of hair, Cell. Mol. Biol. 46 (2000) 1005–1016.
[62] J.L. Bantignies, G.L. Carr, D. Lutz, S. Marull, G.P. Williams, G. Fuchs, Chemical imaging of hair by infrared microspectroscopy using synchrotron radiation, J. Cosmet. Sci. 51 (2000) 73–90.
[63] L. Bertrand, J. Doucet, P. Dumas, A. Simionovici, G. Tsoucaris, P. Walter, Microbeam synchrotron imaging of hairs from ancient Egyptian mummies, J. Synchrotron Radiat. 10 (2003) 387–392.
[64] K.S. Kalasinsky, Drug distribution in human hair by infrared microscopy, Cell. Mol. Biol. (Noisy-le-grand) 44 (1998) 81–87.
[65] D.L. Wetzel, D.N. Slatkin, S.M. Levine, FT-IR microspectroscopic detection of metabolically deuterated compounds in the rat cerebellum: a novel approach for the study of brain metabolism, Cell. Mol. Biol. (Noisy-le-grand) 44 (1998) 15–27.
[66] D.L. Wetzel, A.J. Eilert, L.N. Pietrzak, S.S. Miller, J.A. Sweat, Ultraspatially-resolved synchrotron infrared microspectroscopy of plant tissue in situ, Cell. Mol. Biol. (Noisy-le-grand) 44 (1998) 145–168.
[67] P. Yu, J.J. McKinnon, C.R. Christensen, D.A. Christensen, Imaging molecular chemistry of Pioneer corn, J. Agric. Food Chem. 52 (2004) 7345–7352.
[68] P. Yu, Molecular chemistry imaging to reveal structural features of various plant feed tissues, J. Struct. Biol. 150 (2005) 81–89.
[69] D.L. Wetzel, P. Srivarin, J.R. Finney, Revealing protein infrared spectral detail in a heterogeneous matrix dominated by starch, Vib. Spectrosc. 31 (2003) 109–114.
[70] P. Yu, R. Wang, Y. Bai, Reveal protein molecular structural–chemical differences between two types of winterfat (forage) seeds with physiological differences in low temperature tolerance using synchrotron-based Fourier transform infrared microspectroscopy, J. Agric. Food Chem. 53 (2005) 9297–9303.
[71] K.M. Dokken, L.C. Davis, N.S. Marinkovic, Using SR-IMS to study the fate and transport of organic contaminants in plants, Spectroscopy 20 (2005) 14.
[72] T.K. Raab, M.C. Martin, Visualizing rhizosphere chemistry of legumes with mid-infrared synchrotron radiation, Planta 213 (2001) 881–887.
[73] N.S. Marinkovic, A.R. Adzic, M. Sullivan, K. Kovacs, D.L. Rousseau, S.R. Yeh, M.R. Chance, L.M. Miller, Design and implementation of a rapid-mix flow cell for time-resolved infrared microspectroscopy, Rev. Sci. Instrum. (2000).
[74] N.S. Marinkovic, R. Huang, P. Bromberg, M. Sullivan, J. Toomey, L.M. Miller, E. Sperber, S. Moshe, K.W. Jones, E. Chouparova, S. Lappi, S. Franzen, M.R. Chance, Center for synchrotron biosciences' U2B beamline: an international resource for biological infrared spectroscopy, J. Synchrotron Radiat. 9 (2002) 189–197.
[75] D. Fried, N. Ashouri, T. Breunig, R. Shori, Mechanism of water augmentation during IR laser ablation of dental enamel, Lasers Surg. Med. 31 (2002) 186–193.
[76] L. Beney, Y. Mille, P. Gervais, Death of *Escherichia coli* during rapid and severe dehydration is related to lipid phase transition, Appl. Microbiol. Biotechnol. 65 (2004) 457–464.
[77] D. Carrier, P.T.T. Wong, High-pressure vibrational spectroscopic investigation of biological molecules, Eu. J. Solid State Inorg. Chem. 34 (1997) 733–744.
[78] M. Holtje, T. Forster, B. Brandt, T. Engels, W. von Rybinski, H.D. Holtje, Molecular dynamics simulations of stratum corneum lipid models: fatty acids and cholesterol, Biochim. Biophys. Acta-Biomembr. 1511 (2001) 156–167.
[79] S.Y. Park, R.E. Hannemann, E.I. Franses, Dynamic tension and adsorption behavior of aqueous lung surfactants, Colloids Surf., B 15 (1999) 325–338.
[80] A. Xie, Q. He, L.M. Miller, B. Sclavi, M.R. Chance, Low frequency vibrations of amino acid homo-polymers observed by synchrotron far infrared absorption spectroscopy: excited state affects dominate the temperature dependence of the spectra, Biopolymers 49 (1999) 591–603.
[81] T.R. Globus, D.L. Woolard, A.C. Samuels, B.L. Gelmont, J. Hesler, T.W. Crowe, M. Bykhovskaia, Submillimeter-wave Fourier transform spectroscopy of biological macromolecules, J. Appl. Phys. 91 (2002) 6105–6113.
[82] P. Dumas, L. Miller, Biological and biomedical applications of synchrotron infrared microspectroscopy, J. Biol. Phys. 29 (2003) 201–218.
[83] M. Szczerbowska-Boruchowska, J. Chwiej, M. Lankosz, D. Adamek, S. Wojcik, A. Krygowska-Wajs, B. Tomik, S. Bohic, J. Susini, A. Simionovici, P. Dumas, M. Kastyak, Intraneuronal investigations of organic components and trace elements with the use of synchrotron radiation, X-Ray Spectrom. 34 (2005) 514–520.
[84] L.M. Miller, J. Tibrewala, C.S. Carlson, Examination of bone chemical composition in osteoporosis using fluorescence-assisted synchrotron infrared microspectroscopy, Cell. Mol. Biol. (Noisy-le-grand) 46 (2000) 1035–1044.